Chemical Geology 513 (2019) 143–152

Contents lists available at ScienceDirect

Chemical Geology

journal homepage: www.elsevier.com/locate/chemgeo

# Boron isotope composition of the cold-water coral *Lophelia pertusa* along the Norwegian margin: Zooming into a potential pH-proxy by combining bulk and high-resolution approaches

Hana Jurikova[a], Volker Liebetrau[a,*], Jacek Raddatz[b], Jan Fietzke[a], Julie Trotter[c], Alexander Rocholl[d], Stefan Krause[a], Malcolm McCulloch[e], Andres Rüggeberg[f], Anton Eisenhauer[a]

[a] GEOMAR Helmholtz Centre for Ocean Research Kiel, Wischhofstr. 1-3, 24148 Kiel, Germany
[b] Institute of Geosciences, Goethe-University Frankfurt, Altenhöferallee 1, 60438 Frankfurt am Main, Germany
[c] School of Earth Sciences and UWA Oceans Institute, The University of Western Australia, Crawley, Australia
[d] GFZ German Research Centre for Geosciences – Helmholtz Centre Potsdam, Telegrafenberg, 14473 Potsdam, Germany
[e] Oceans Graduate School, UWA Oceans Institute, and ARC Centre of Excellence for Coral Reef Studies, The University of Western Australia, Crawley, Australia
[f] Department of Geosciences, University of Fribourg, Chemin du Musée 6, 1700, Fribourg, Switzerland

ARTICLE INFO

Michael E. Böttcher

*Keywords:*
Isotope geochemistry
Ocean acidification
pH and carbon cycle reconstruction
Biomineralisation
Aragonite precipitation
Diagenesis
MC-ICP-MS
SIMS
Laser ablation

ABSTRACT

High-latitude cold-water coral reefs are particularly vulnerable to climate change due to enhanced $CO_2$ uptake in these regions. To evaluate their physiological functioning and potential application as pH archives, we retrieved both recent and fossil samples of *Lophelia pertusa* along the Norwegian margin from Oslofjord (59°N), over to Trondheimsfjord, Sula and Lopphavet (70.6°N). Boron isotope analyses ($\delta^{11}B$) were undertaken using solution-based and laser ablation multi-collector inductively coupled plasma mass spectrometry (MC-ICP-MS; LA-ICP-MS), and secondary ion mass spectrometry (SIMS). Epi-fluorescence microscopy was employed to provide a rapid pre-screening routine for structure-specific subsampling in the coral skeleton. This integrated approach enabled us to assess heterogeneities within single specimens, as well as to investigate the role of local environmental influences including recent and past variations. All three mass spectrometry methods show substantial differences in the $\delta^{11}B$ of the theca wall (TW) and the centres of calcification (COC's). Micro-bulk subsamples milled from the theca wall of modern specimens originating from different habitats but with comparable seawater pH (8–8.16) gave consistent $\delta^{11}B$ values averaging 26.7 ( ± 0.2‰, 2σ, $n = 4$), while COC subsamples systematically deviated towards lower B/Ca (by ~40%) and depleted $\delta^{11}B$ values (minimum 22.7 ± 0.3‰, 2σ), implying a difference of at least 4‰ between TW and COC. SIMS and LA-ICP-MS measurements identified much larger internal heterogeneities with maximum variation of ~10‰ between the distinct skeletal structures; minimal SIMS $\delta^{11}B$ values of ~17.3 ± 1.2‰ (2σ) were associated with the pure COC material. Our findings may be interpreted in terms of the occurrence of two main, but likely different, biomineralisation mechanisms in *L. pertusa*, with the COC's generally exhibiting minimal pH up-regulation, potentially supporting the use of bicarbonate in the early stages of biomineralisation. Furthermore, we highlight the potential utility of *L. pertusa* for palaeo-proxy studies if targeting the compositionally homogenous TW zones devoid of COC admixtures, which appear to provide highly reproducible measurements.

## 1. Introduction

Anthropogenic increase in atmospheric carbon dioxide ($CO_2$) concentrations has contributed to the decrease of surface ocean pH by ~0.1 since the industrial revolution, and it is predicted to further decrease by at least 0.3 units by the end of this century (IPCC, 2013; Orr et al., 2005; Caldeira and Wickett, 2003). Associated decrease in seawater carbonate saturation state (Ω) poses a particular threat to marine calcifying organisms as it impairs their biomineralisation processes (e.g. Silverman et al., 2009; Krief et al., 2010; McCulloch et al., 2012a). Carbon dioxide uptake is enhanced at high-latitudes, with the subpolar North Atlantic region being a major $CO_2$ sink (e.g. Bates and Mathis, 2009; Halloran et al., 2015), making the high-latitude cold-water coral reefs especially vulnerable to climate change (Büscher et al., 2017; Guinotte et al.,

* Corresponding author.
*E-mail address:* vliebetrau@geomar.de (V. Liebetrau).

https://doi.org/10.1016/j.chemgeo.2019.01.005
Received 5 October 2018; Received in revised form 21 December 2018; Accepted 10 January 2019
Available online 14 January 2019

2006; Raddatz et al., 2016). The deep-sea scleractinian coral *Lophelia pertusa* (Linnaeus, 1758) is the most common framework forming coral in the northeastern Atlantic, supporting > 1300 associated species (e.g. Freiwald et al., 2004; Roberts et al., 2006). Its wide geographical distribution and extensive skeletal mass provides sufficient quantities of material for precise dating and proxy-applications as well as a highly advantageous cosmopolitan archive of environmental conditions. Given that *L. pertusa* is a relatively slow growing azooxanthellate species (~25 mm per year; Gass and Roberts, 2011), potential kinetic effects are minimal and it is not subjected to the confounding vital effects of symbionts that occur in other coral groups (e.g. Hönisch et al., 2003; Al-Horani et al., 2003; Trotter et al., 2011; Vielzeuf et al., 2018). Cold-water deep-sea corals can live for hundreds of years, so they can provide a unique window into long-term environmental changes in the deep-ocean at a resolution that rivals ice cores (Adkins et al., 2004; Houlbrèque et al., 2010). These attributes have over recent years made them attractive candidates for palaeo-proxy research (e.g. Montagna et al., 2014; Raddatz et al., 2013, 2014a; Rüggeberg et al., 2008; Cohen et al., 2006). Moreover, we can use these corals to investigate their physiological responses to environmental change, which are important for predicting how these organisms and the wider ecosystems will respond to future climatic changes.

Boron isotope ($\delta^{11}B$) composition of marine biogenic calcium carbonate is regarded as the most reliable pH-proxy as it reflects the pH of fluid from which it precipitated (e.g. Vengosh et al., 1991; Hemming and Hanson, 1992; Sanyal et al., 2000; see Section 1.1 below for further details on the principles of the $\delta^{11}B$-pH proxy). This can be either seawater and/or calcifying fluid, which makes $\delta^{11}B$ a versatile tracer for ocean and internal carbonate chemistry (Hönisch et al., 2004; McCulloch et al., 2012b; Trotter et al., 2011; Anagnostou et al., 2012; Stewart et al., 2016; Tanaka et al., 2015). Boron concentrations are much higher in aragonitic deep-sea corals (up to 100 ppm; e.g. Douville et al., 2010) compared to other calcifiers, such as tropical corals (~50 ppm; e.g. Hemming and Hanson, 1992), brachiopods (~35 ppm; e.g. Jurikova et al., 2019), and foraminifera (~10 ppm; Rae et al., 2011). The high boron concentrations of the deep-sea corals permit precise $\delta^{11}B$ analyses from small samples sizes which, together with their potential for providing continuous records at (sub)decadal to centennial time-scales, makes them a promising archive for $\delta^{11}B$-pH reconstructions. While it seems to be possible to derive robust records of seawater pH from coral skeletons (e.g. Douville et al., 2010; Wei et al., 2009; Liu et al., 2009), there is a growing evidence that physiological and biomineralisation processes provide significant uncertainties in translating $\delta^{11}B$ values to seawater pH. As observed in other corals, *L. pertusa* appears to pose a strong biological control over its calcification by up-regulation of internal pH of its calcifying fluid, which results in a reduced $\delta^{11}B$ sensitivity to seawater pH (Blamart et al., 2007; McCulloch et al., 2012b; Rollion-Bard et al., 2010; Rollion-Bard et al., 2011; Wall et al., 2015). This may contribute to the ability of *L. pertusa* to thrive in waters often undersaturated with respect to aragonite ($\Omega_{arg}$), but leaves unanswered questions on their application as potential pH-recorders. By fully understanding their internal $\delta^{11}B$ heterogeneities, variations between individuals and their responses to environmental conditions, we may be able to decipher the processes that govern the incorporation of boron into their skeleton.

Here we report new $\delta^{11}B$ and B/Ca data determined from several modern as well as fossil *L. pertusa* specimens collected off the coast of Norway, which are combined with published data from Raddatz et al. (2016). Our sampling sites included environments characteristic of very different local settings; the southern Oslofjord is located close to brackish conditions of the Baltic Sea outflow water and is influenced by seasonal variations, the mid-latitude Sula reef is located within open-water conditions, while Trondheimsfjord at a comparable latitude is a sheltered and exceptionally shallow water habitat, and finally Lopphavet that presents the northernmost flourishing coral reef. We compare these recent samples to a ~5 ka old *L. pertusa* from Oslofjord, a ~10 ka sample from Lopphavet, and a ~100 ka specimen from Challenger Mound (IODP Site U1317; Raddatz et al., 2014b). This allowed for a detailed assessment of the $\delta^{11}B$-proxy in *L. pertusa* that grew under very different natural conditions. We employ conventional bulk-sample solution-based MC-ICP-MS, as well as high-resolution *in situ* techniques using SIMS and LA-ICP-MS, to investigate the $\delta^{11}B$ distribution within skeletal structures on different spatial scales, and to evaluate heterogeneities within single specimens. Finally, we compare the various $\delta^{11}B$ datasets to assess the utility of *L. pertusa* as a pH archive, its physiological and biomineralisation responses to ambient changes, and the potential influence of diagenesis on the preservation of the fossil samples.

### 1.1. Principles of the boron isotope pH-proxy

Boron in seawater is present as either trigonal boric acid [$B(OH)_3$] or tetrahedral borate ion [$B(OH)_4^-$]. The speciation of these two forms is pH dependent, which means that the relative abundance of borate ion increases with pH, while boric acid decreases, and vice versa. Moreover, the isotopic composition of each species changes as a function of pH, with borate ion preferentially taking the lighter $^{10}B$ and boric acid the heavier $^{11}B$ isotope. A pronounced fractionation exists between the two boron species (27.2‰; Klochko et al., 2006; Nir et al., 2015) and in theory allows for precise pH calculation from measurements of $\delta^{11}B$ of either of the species (Vengosh et al., 1991; Hemming and Hanson, 1992; Zeebe, 2005; Klochko et al., 2006). The fundamental assumption for the proxy application is that borate ion is the only species incorporated into marine calcifiers. This was shown by Vengosh et al. (1991) and Hemming and Hanson (1992), who observed a large offset between the boron isotope composition of seawater and marine carbonates, which were found to be closer to the composition of borate ion (at seawater pH). The exclusive incorporation of borate ion into carbonates has been recently challenged by observations documenting the presence of the trigonal species in carbonates using nuclear magnetic resonance and electron-loss spectroscopy (Klochko et al., 2009; Rollion-Bard et al., 2011). However, with ongoing discussions a possible explanation for this might be a crystallographic control on the modification of boron structure within the crystal lattice of calcite or aragonite (while $\delta^{11}B$ is maintained), and not the assimilation of boric acid (Rasbury and Hemming, 2017). Regardless, many studies have revealed a strong control of pH on $\delta^{11}B$ in inorganic synthesized carbonates, which for aragonite is consistent with the uptake of the borate species (e.g. Uchikawa et al., 2015; Kaczmarek et al., 2016). For biologically mediated marine carbonates, contrasting results have been published. Three different groups of marine calcifiers have been identified according to their $\delta^{11}B$ compositions: 1) those with no or minimal offset to the theoretical $\delta^{11}B_{borate}$ curve such as benthic foraminifera (e.g. Rae et al., 2011); 2) those recording $\delta^{11}B$ above the expected theoretical $\delta^{11}B_{borate}$ line including symbiont-bearing planktonic foraminifera, cold and warm-water scleractinia, coralline red algae or brachiopods (e.g., Hönisch et al., 2003; McCulloch et al., 2012a, 2012b; Fietzke et al., 2015; Jurikova et al., 2019); and 3) those below the borate curve such as non-symbiont bearing planktonic foraminifera or aragonitic benthic foraminifera (e.g. Martínez-Botí et al., 2015; Rae et al., 2011). We note, however, that such generalisation is not straightforward and caution should be employed when interpreting offsets. This is highlighted by recent findings on a symbiont-bearing foraminifera that apparently records $\delta^{11}B$ below the inorganic $\delta^{11}B_{borate}$ line, contrary to expectations (Henehan et al., 2016). The offsets relative to the theoretical $\delta^{11}B_{borate}$ curve can be explained by biological processes ('vital effects'), and may be calibrated by culture experiments or core-top assessments. However, the $\delta^{11}B$ values of numerous scleractinian cold-water corals are significantly above the inorganic $\delta^{11}B_{borate}$ equilibrium line. In line with biomineralisation models (Al-Horani et al., 2003; Marubini et al., 2008), this indicates a strong pH up-regulation of the internal calcifying fluid against ambient seawater

pH (e.g. McCulloch et al., 2012b; Anagnostou et al., 2012; Ries, 2011), further complicating their use as seawater pH archives. With a ΔpH of 0.6 to 0.8 units (above seawater), this offset appears to be higher in cold-water corals than in tropical corals (with ΔpH of 0.2–0.4, Hönisch et al., 2003), and will be difficult to maintain under decreasing seawater pH. In the aragonitic corals, changes in the internal pH of the calcifying fluid are generally ~⅓ to ½ of those in ambient seawater pH, which translates to an energetic cost of about 10% per 0.1 unit decrease of seawater pH (Trotter et al., 2011; McCulloch et al., 2012b). These observations cast doubts on the ability of cold-water azooxanthellae corals to calcify and, ultimately, survive under reduced ocean pH conditions, especially when combing acidification scenarios with additional thermal stress and/or nutrient limitations.

## 2. Materials and methods

### 2.1. Sample material

Samples were recovered during the research cruise POS 391 onboard R/V Poseidon off the coast of Norway in 2009. Recent *L. pertusa* specimens were collected with minimal invasion using the manned submersible JAGO (GEOMAR, Kiel) at Lopphavet and Oslofjord, and with a Van-Veen grab at the Sula reef complex (Fig. 1). The deep-water samples from Trondheimsfjord were collected onboard R/V VITA using ROV MINERVA (Røberg, 63°28′36″N, 9°59′43″W; 240 m depth, temperature 8.1 °C, and salinity 31.2). Fossil Holocene samples were retrieved using gravity and box corers in the vicinity of the cold-water reefs at Lopphavet (between 70°26.6′N–70°28.9′N and 21°10.2′E–21°11.4′E, core numbers: 551–2, 551–3, 557–3, 559–2, and 559–3) at a depth between 226 and 268 m, and in Oslofjord (59.08′N, 19.5′E, core numbers: 575–2, 578–1, 576–1, and 576–2) at 100 m water depth. Prior to sample selection, sediment cores were frozen and cut to avoid disturbance following Dorschel et al. (2005). Coral samples were first washed, rigorously cleaned from potential secondary surface stains and coatings with a dental drill down to massive primary aragonite, and subsequently cut for further subsampling. For bulk analyses, sections perpendicular to growth axis were subsampled using a dental drill and a New Wave micromill in different areas of the skeleton (TW and COC; Fig. 2) following Raddatz et al. (2016). One recent sample from Lopphavet was vacuum embedded using epoxy resin and polished for SIMS measurements. Samples for LA-ICP-MS were fixed using a two component, cold embedding (epoxy-stick, saBesto, Würth) that does not penetrate into the sample. Epi-fluorescence microscope imaging was undertaken using a Zeiss stereomicroscope Discovery V8 with DAPI filter set, equipped with an AxioCam MRm Rev.3. The ZEN 2.3 software package was used for image acquisition.

### 2.2. Isotopic and elemental analyses

Bulk solution-based boron isotope analyses were carried out on a NU Plasma II MC-ICP-MS at the University of Western Australia (UWA) following the protocols described in McCulloch et al. (2014). Briefly, about 5 mg of sample powder material was first cleaned to remove organic material by sonication in dilute hypochlorite (~7% NaOCl). Subsequently, samples were rinsed in a series of steps using ultrapure Milli-Q to remove residual bleach solution. Cleaned powders were dissolved in 0.5 M $HNO_3$. An aliquot was used for major and trace element analyses, measured on a Thermo X-Series II quadrupole ICP-MS at the University of Western Australia, and referenced to the international carbonate (*Porites*) standard JCp-1 (Okai et al., 2002), giving a long-term reproducibility for B/Ca within ± 10% and ± 2% for Mg/Ca (RSD, 2σ). The remaining aliquot was processed for boron separation using combined cation and anion chromatography. The boron isotope composition of the purified B eluent was analysed in ~0.15 M $HNO_3$. The $^{11}B/^{10}B$ ratios are expressed in standard delta notations in per mille (‰) relative to the reference material NIST SRM 951 boric acid (Catanzaro et al., 1970) as follows $\delta^{11}B\,(‰) = [(^{11}B/^{10}B_{sample})/(^{11}B/^{10}B_{standard}) - 1] \times 1000$. The veracity of the MC-ICP-MS procedure is demonstrated using a gravimetrically prepared standard UWA24.7 relative to NIST SRM 951, which gives values consistent with gravimetry ($\delta^{11}B = 24.7 \pm 0.3‰$, 2σ) for solutions ranging in concentration from 50 to 500 ppb, equivalent to 2–10 mg of coral sample. Each sample or standard was run twice in a sequence with the average value reported. The standard deviation (2σ) between the runs ranged between ± 0.00‰ and ± 0.31‰. Our data is reported with the more conservative uncertainty of ± 0.34‰, based on repeated

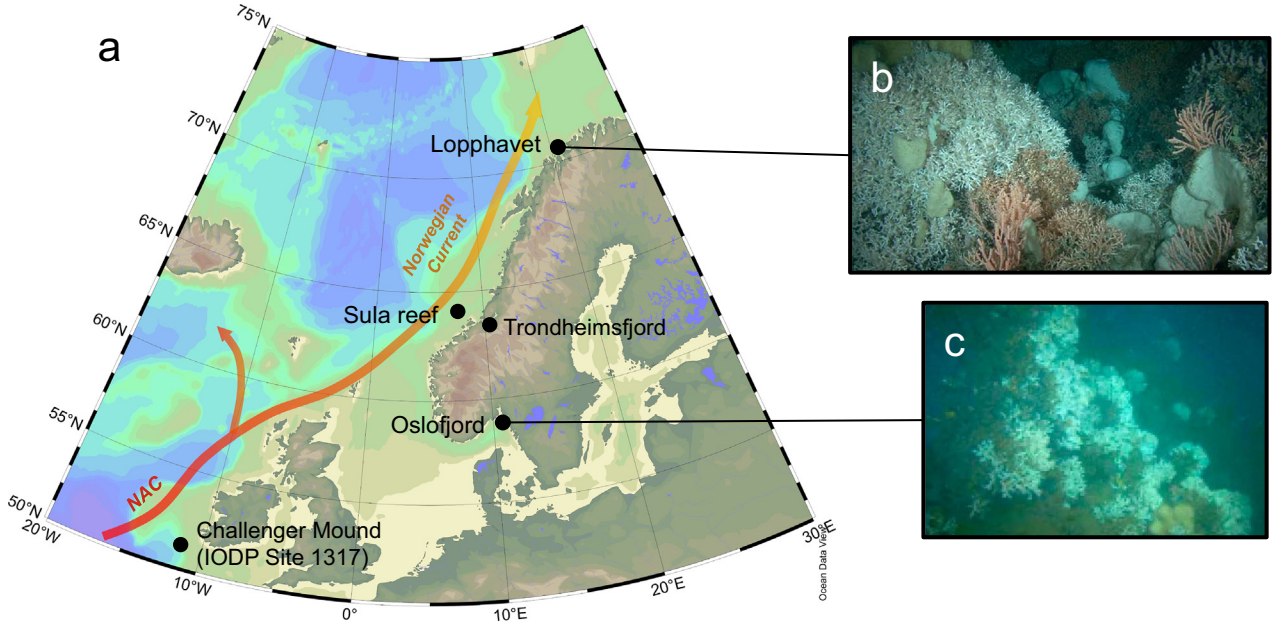


**Fig. 1.** a) Study location map of recent flourishing deep-sea coral reefs off the coast of Norway. These ecosystems thrive along the warm North Atlantic Current (NAC), which later forms the Norwegian Current (map generated using ODV; Schlitzer, 2016); b) close up of the northernmost Lopphavet reef, and c) brackish Oslofjord reef. are from cruise POS 391 cruiseUnderwater photos were taken during the the POS 391 cruise using a manned submersible JAGO (from Raddatz et al., 2016). (For interpretation of the references to color in this figure, the reader is referred to the web version of this article.)

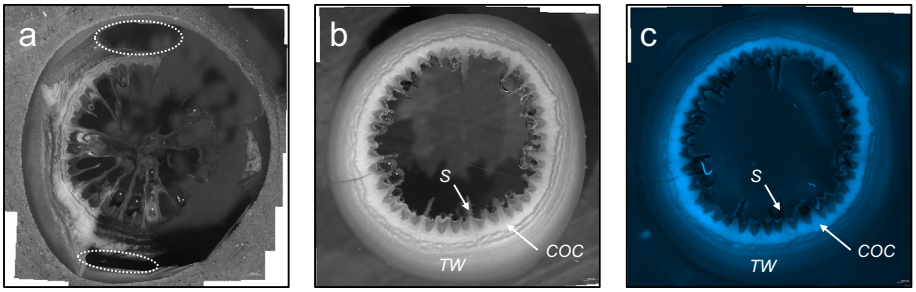


**Fig. 2.** Mosaic of binocular microscope images of polished transverse sections in a recent *L. pertusa* from Lopphavet; a) underside view after milling for micro-bulk samples (theca wall in grey and COC in white). Note the fine interlayering and the detailed septal growth structures, the tracks of computer-assisted micromilling (sharp black horizontal contours in bottom of image), and the efficient but imprecise handheld dental-drill milling (irregular horizontal track in top part of image). b) Upside view of an older and more solid counterpart, with visible later stage structural changes of septa; c) same as in panel 'b' with epi-fluorescence (EGFP1) image illustrating the different biomineralisation structures. (For interpretation of the references to color in this figure, the reader is referred to the web version of this article.)

measurements of the coral standard JCp-1 ($\delta^{11}B = 24.3 \pm 0.34‰$, 2σ; McCulloch et al., 2014), consistent with values reported by other laboratories (Jurikova et al., 2019; Wang et al., 2010).

High spatial resolution $\delta^{11}B$ profiles were obtained *in situ* by SIMS and LA-ICP-MS. SIMS analyses were performed at the GFZ Potsdam using a large geometry CAMECA 1280-HR SIMS instrument as described in Büttner et al. (2016). Analyses employed a 5 nA $^{16}O$-primary beam focused to a ~20 µm diameter at the polished sample surface. Instrument calibration was based on the inorganic calcite standard reference material UWC-1 (Kasemann et al., 2009). Final values were converted to a common scale and are reported against NIST 951. The analytical repeatability for $\delta^{11}B$ was better than ± 1.2‰ (2σ, N = 4). LA-ICP-MS measurements were undertaken at GEOMAR, Kiel on an AXIOM MC-ICP-MS connected to an ESI New Wave Research UP193FX excimer laser ablation system equipped with a large format cell, following the protocols of Fietzke et al. (2010). For instrument calibration we used the soda-lime glass standard NIST SRM 610, with final values expressed relative to NIST 951. The analytical reproducibility for laser $\delta^{11}B$ values was better than ± 1.0‰ (2σ).

pH values were derived from boron isotope data using the standard equation:

$$pH = pK_B^* - \log\left[-\frac{\delta^{11}B_{sw} - \delta^{11}B_{borate}}{\delta^{11}B_{sw} - (^{11-10}K_B \times \delta^{11}B_{borate}) - 10^3\,(^{11-10}K_B - 1)}\right]$$

where $\delta^{11}B_{sw}$ is the isotopic composition of seawater (39.61‰; Foster et al., 2010), $^{11-10}K_B$ is the isotope fractionation factor between borate ion and boric acid (1.0272 ± 0.0006; Klochko et al., 2006), and $pK_B^*$ is the dissociation constant for boric acid at *in situ* temperature, salinity and pressure (Dickson, 1990; Millero, 1979). For the Norwegian *L. pertusa* samples we used a value of $pK_B^* = 8.81$ based on the mean local temperature 7 °C and salinity 35 (Raddatz et al., 2016; Flögel et al., 2014). To translate the $\delta^{11}B$ values recorded in the coral skeleton of *L. pertusa* to pH units, we assume that only $\delta^{11}B_{borate}$ is incorporated ($\delta^{11}B_{coral} = \delta^{11}B_{borate}$) and that no further fractionation occurs during calcification.

## 3. Results

### 3.1. Solution-based bulk boron isotope data

Our solution-based bulk $\delta^{11}B$ data are summarised in Table 1. With this approach we compare three different microstructural components: 1) theca, material exclusively milled in the outer theca wall; 2) COC (centres of calcification or early mineralisation zone; e.g. Cuif and Dauphin, 2005); and 3) by purpose mixed – gross bulk integrating theca as well as COC. Note that isolating material exclusively from COC is challenging because of spatial limitations (Fig. 2). The fluorescence microscopy provided a fast pre-screening routine for subsampling the specific microstructural components (Figs. 2 and 3). This exercise was performed on a recent *L. pertusa* from four different locations (from south to north): Oslofjord, Trondheimsfjord, Sula and Lopphavet as well as several fossil specimens. The $\delta^{11}B$ composition of the recent theca material did not vary geographically, recording a narrow range between 26.5 and 26.8‰ regardless of environmental settings, highly consistent within the analytical uncertainties (Table 1). While some of the key physical properties are comparable between the different reef sites (salinity ~35.1, temperature ~6–7 °C, pH ~8–8.16), they are subjected to distinct environmental influences. For instance, Oslofjord, located close to the brackish conditions of the Baltic Sea outflow experiences the strongest seasonal variations, Trondheimsfjord presents sheltered shallow water habitat whereas Sula is open-water, and finally Lopphavet represents the northernmost flourishing reef at the biogeographical limit of coral occurrence. Conversely, the theca wall $\delta^{11}B$ composition of the fossil sample from Oslofjord (~4.6 ka BP; kiloannum before present) was 25.1‰, > 1.5‰ lower than the present day values (26.5–26.8‰). The Early Holocene sample (~10.1 ka BP) from Lopphavet gave a $\delta^{11}B$ of 26.1‰ in the theca wall, which is about 0.5‰ lower in comparison to the modern specimens. Finally, the oldest sample (Late Pleistocene, ~104 ka BP) from Challenger Mound recorded the highest $\delta^{11}B$ value of 27.4‰, > 0.5‰ higher than the upper $\delta^{11}B$ values for recent corals.

COC-dominated subsamples (assessed by fluorescence microscopy, and referring to a considerable prevalence of COC material over theca, however not exclusively COC due to the limited spatial resolution of the bulk approach; Fig. 2) were obtained from the recent and the Early Holocene *L. pertusa* from Lopphavet. Generally, the COC material was depleted in $^{11}B$ relative to the theca wall, with $\delta^{11}B$ values of 22.7‰ and 25.8‰ measured in the modern and the fossil sample, respectively. When compared to the corresponding theca $\delta^{11}B$ values (26.6‰ and 26.1‰), this indicates a substantial internal heterogeneity of at least 4‰ for the recent coral, and only minor internal variations of about 0.4‰ in the fossil Holocene specimen.

### 3.2. SIMS boron isotope profile

In order to assess the influence of micro-scale $\delta^{11}B$ heterogeneities, we conducted selective ion spot analyses on a polished surface of *L. pertusa*. For this we used the recent *L. pertusa* specimen from Lopphavet reef. The ion spots were organised consecutively, profiling the skeleton from the innermost calyx wall, over the septum and COC region, to the outermost theca wall (Fig. 4). At high spatial resolution the internal $\delta^{11}B$ variations were much larger, almost 10‰ in contrast to the 4‰ measured in bulk subsamples. In the inner skeletal region and within the septum, the $\delta^{11}B$ was comparatively light, with values around ~23‰. The outermost theca material had the highest and very consistent $\delta^{11}B$ values (five outer ion spots measurements: number 13–17 in the blue skeletal structures; Fig. 4), resulting in an average $\delta^{11}B$ for theca of ~26‰ ( ± 0.6‰, 1σ, $n = 5$). This is also in good agreement with the theca $\delta^{11}B$ values from solution-based bulk analyses (26.6‰; Fig. 5). Lowest values were obtained from the COC areas (brown skeletal structures, Fig. 4) with measured $\delta^{11}B$ values as low as ~17‰, much lower than measurements of the impure COC fractions with the bulk approach.

**Table 1**
Solution-based $\delta^{11}B$ values, calculated pH, and B/Ca ratios for *L. pertusa* recovered off the coast of Norway on Research Cruise POS 391. Subsample refers to the different skeletal microstructures, with theca representing the pure theca wall aragonite, COC (centre of calcification) is dominated by COC and septa (but not entirelly pure), and mixed being the gross bulk fraction integrating the mixed skeletal composition (theca, COC and septa). Data of samples marked with asterisk (*) are taken from Raddatz et al. (2016; refer to sampling site coordinates therein). The last sample, marked with a plus sign (+), is from a coral mound Challenger (IODP Site U1317; Raddatz et al., 2014b) in the Northern Atlantic and implemented into this study for a comparison as a well-preserved sample, with very different origin and age. Note that to stay in subsampling target and to keep the theca wall content as pure as possible without contribution from other skeletal structures, the micro-milled material for this sample was < 1 mg total mass.

| Lab code | Location | Latitude | Longitude | U/Th age (ka) | Water depth (m) | Sub-sample | $\delta^{11}B$ (‰) ± 0.34 (2σ) | Calcul. pH | B/Ca (μmol/mol) ± 10% (RSD, 2σ) | Mg/Ca (mmol/mol) ± 2% (RSD, 2σ) |
|---|---|---|---|---|---|---|---|---|---|---|
| 821–13* | Oslofjord | 59°04 N | 10°44 E | 4.61 ± 0.04 | 100 | Theca | 25.10 | 8.78 | 566 | 3.75 |
| 822–13* | Oslofjord | 59°04 N | 10°44 E | 3.94 ± 0.03 | 100 | Theca | 26.83 | 8.89 | 696 | 3.56 |
| 431–11* | Oslofjord | 59°04 N | 10°44 E | Recent | 100 | Theca | 26.82 | 8.89 | 863 | 4.07 |
| 435–11 | Trondheimsfjord | 63°35 N | 10°31 E | Recent | 40 | Theca | 26.66 | 8.88 | 748 | 4.23 |
| 436–11 | Trondheimsfjord | 63°35 N | 10°31 E | Recent | 40 | Mixed | 25.46 | 8.80 | 671 | 5.06 |
| 434–11 | Trondheimsfjord | 63°28 N | 09°59 E | Recent | 240 | Mixed | 25.44 | 8.80 | 746 | 3.46 |
| 433–11* | Sula | 64°05 N | 08°05 E | Recent | 290 | Theca | 26.53 | 8.87 | 823 | 3.96 |
| 433–11(b) | Sula | 64°05 N | 08°05 E | Recent | 290 | Mixed | 25.08 | 8.78 | 712 | 4.07 |
| 432–11 | Sula | 64°05 N | 08°05 E | Recent | 290 | Mixed | 24.99 | 8.77 | 735 | 3.91 |
| 439–11* | Lopphavet | 70°26 N | 21°10 E | 10.07 ± 0.11 | 260 | Theca | 26.13 | 8.84 | 608 | 3.86 |
| 440–11* | Lopphavet | 70°26 N | 21°10 E | 10.07 ± 0.11 | 260 | COC | 25.76 | 8.82 | 534 | 4.10 |
| 440–11(b) | Lopphavet | 70°26 N | 21°10 E | 10.07 ± 0.11 | 260 | Mixed | 25.83 | 8.82 | 584 | 4.18 |
| 429–11* | Lopphavet | 70°26 N | 21°10 E | Recent | 230 | Theca | 26.60 | 8.87 | 792 | 3.63 |
| 430–11 | Lopphavet | 70°26 N | 21°10 E | Recent | 230 | COC | 22.65 | 8.62 | 579 | 4.12 |
| 428–11 | Lopphavet | 70°26 N | 21°10 E | Recent | 230 | Mixed | 26.25 | 8.85 | 728 | 4.26 |
| 437–11+ | Challenger Md. | 52°23 N | 11°43 W | 104 ± 2 | 800 | Theca | 27.44 | 8.93 | – | – |

### 3.3. LA-ICP-MS profiles

As a second high-resolution technique we employed laser ablation (LA-ICP-MS), which in contrast to SIMS permits continuous $\delta^{11}B$ profiling and minimal sample preparation. We carried out two $\delta^{11}B$ laser profiles; one on the same specimen as the SIMS analyses – the recent sample from Lopphavet reef, and another one on the Early Holocene specimen from the same location. Both profiles traversed the skeleton from the innermost calyx to the outermost theca wall rim (Fig. 6). Notably, the absolute $\delta^{11}B$ values determined with this method differed substantially from the bulk and SIMS values, as well as between the two samples. The relative $\delta^{11}B$ variability, however, agreed very well with the data from SIMS, recording a maximum $\delta^{11}B$ amplitude of ~10‰ in the recent specimen. On the other hand, the internal $\delta^{11}B$ variations were much smaller in the fossil sample, with a maximum internal heterogeneities of ~5‰ between the different skeletal parts.

As also evident from B/Ca ratio (Table 1) and SIMS $^{11}B$ signal (Fig. 5), higher boron content was found within the theca wall, whereas COC and septa were generally depleted in boron in both modern and fossil samples. In contrast to the bulk and SIMS results, no particular trend between laser-based $\delta^{11}B$ values and the different biomineralisation structures was observed, with apparently variable $\delta^{11}B$ compositions occurring in the COC regions as well as the theca wall (Fig. 6).

## 4. Discussion

### 4.1. Biomineralisation of L. pertusa

Scleractinian corals, including *L. pertusa*, are generally understood to calcify in a two-step growth mode (Cuif and Dauphin, 2005; Meibom et al., 2006), although it should be noted that as any model this only presents an oversimplification of the complex biomineralisation

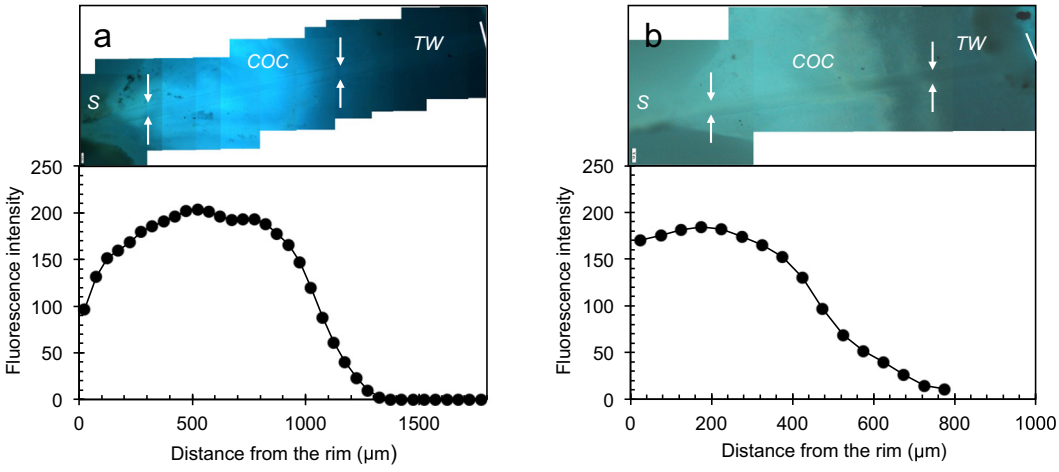


**Fig. 3.** Fluorescence microscope images for; a) recent *L. pertusa*, and b) fossil Holocene *L. pertusa* specimen. Both samples are from the Lopphavet reef. Upper panels show imaged fluorescence (light blue or green colours) across each sample from the innermost to the outermost areas (marked with a white line). A laser ablation track is also visible, indicated by white arrows. Lower panes show the corresponding fluorescence intensities. Note the different x-scales as the fossil sample was smaller in diameter than the recent coral. S – septum, COC – centre of calcification, TW – theca wall. (For interpretation of the references to colour in this figure legend, the reader is referred to the web version of this article.)

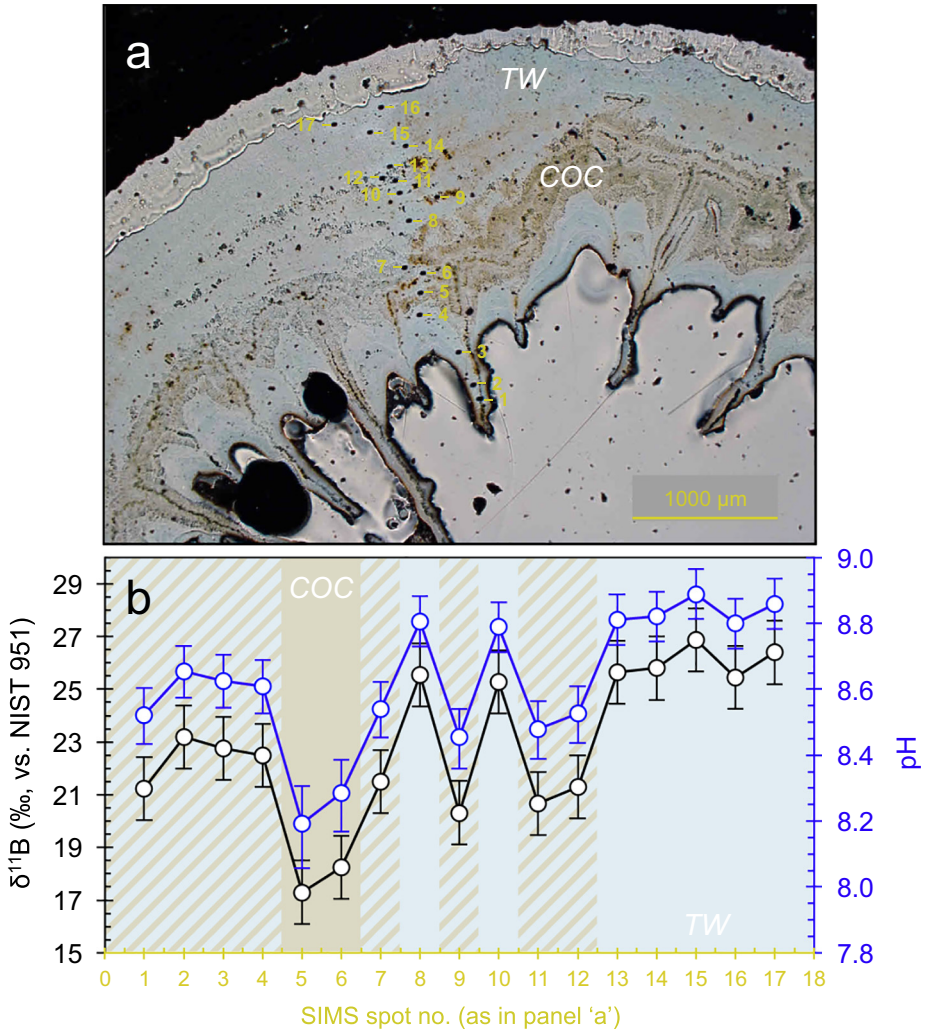


**Fig. 4.** SIMS $\delta^{11}B$ profile across a recent *L. pertusa* specimen from Lopphavet; a) microscope image showing the position of the ion spots; b) $\delta^{11}B$ profile (in black) and calculated pH (in blue) from the innermost (left) to the outermost (right) skeletal region. Brown bars represent measurements entirely within COC – centres of calcification and septa, light blue in pure theca wall (TW) material, and brown-blue diagonal hatching indicates ion spots with likely contribution of both skeletal structures (COC and TW). The analytical repeatability for SIMS $\delta^{11}B$ measurements was ± 1.2‰ (2σ, N = 4), indicated by the error bars.

processes. The COC (or early mineralisation zone) is the primary area of calcification at the growing tips of structural units. The inner calyx wall is built by associated radial septa joined by a complete COC ring. The second step consists of thickening of the septa and calyx by development of aragonite crystals surrounding these structures (Cuif and Dauphin, 2005; Gass and Roberts, 2011). This suggests that two different mechanisms are responsible for each of the key growth steps, which is also reflected in their chemical composition. Our solution-based bulk measurements alone identify at least 4‰ difference in $\delta^{11}B$ between theca and COC, with significant differences in B/Ca and Mg/

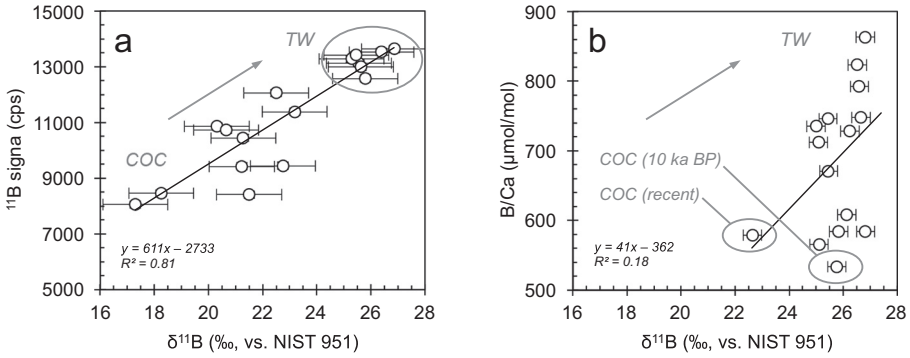


**Fig. 5.** a) SIMS boron isotope data from a recent *L. pertusa* specimen from Lopphavet plotted as $^{11}B$ signal (counts per second, cps) over $\delta^{11}B$. Ion spots located in the theca wall (TW) show highest boron concentration and $\delta^{11}B$ values, in contrast to spots measured in the centres of calcification (COC's) or close to the septa; b) solution-based micro-bulk boron data from all measured *L. pertusa* samples (see Table 1). Here the TW represents the pure theca wall aragonite and COC is the fraction dominated by COC and septal material (but not entirely pure). Mixed samples represent the gross bulk fraction and integrate both TW and COC's. Solid black lines show the least squares linear regressions. Note the differences in the $\delta^{11}B$ analytical reproducibility between approaches; for SIMS the repeatability was ± 1.2‰ (2σ), and for bulk solution-based MC-ICP-MS analyses ± 0.34‰ (2σ).

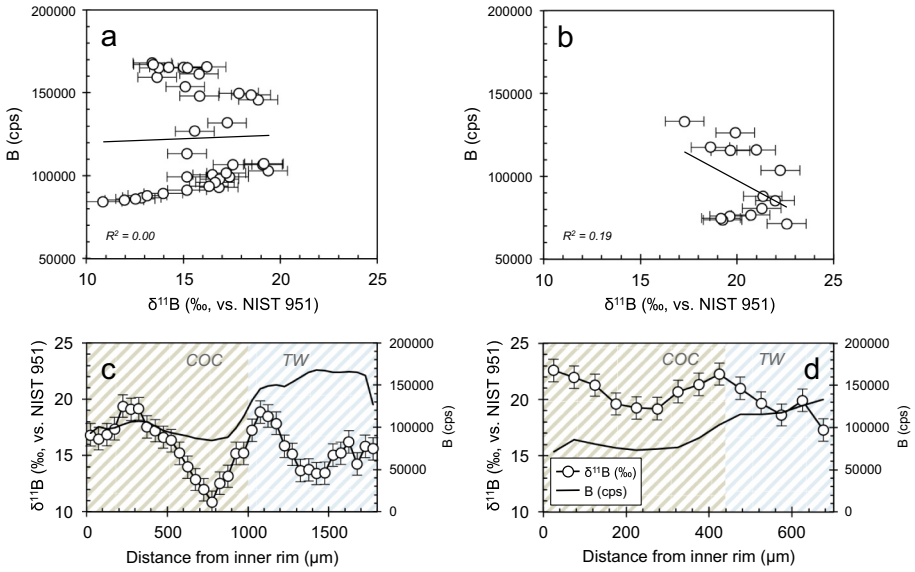


**Fig. 6.** LA-ICP-MS boron data; a) boron concentration (cps) and $\delta^{11}B$ cross-plots for a recent *L. pertusa*, and; b) a fossil Holocene *L. pertusa* from Lopphavet; c) laser ablation profile from the innermost (left) to the outermost (right) skeleton region for the recent, and d) the fossil sample. Unlike for SIMS, it is not straightforward to associate each laser data point with a specific skeletal structure, hence the light diagonal hatching. Generally, brown-white pattern illustrates skeletal areas mainly with COC's and blue-white areas dominated by TW, as also illustrated by epi-fluorescence imaging in Fig. 3 (influence from admixtures, however, cannot be excluded). Note that the analytical reproducibility for LA-ICP-MS $\delta^{11}B$ measurements was ± 1.0‰ (2σ).

Ca concentrations (Table 1). The early COC's have high Mg/Ca but low B/Ca and light $\delta^{11}B$ values, whereas the secondary theca crystals are enriched in $^{11}B$ and almost twice the boron content, suggesting that each growth step is formed from a reservoir of different pH. These $\delta^{11}B$ values for COC should, however, be considered as maximum values, since at least a small contribution from theca crystals is expected due to the limited spatial resolution of subsampling using the bulk approach. By comparing bulk analyses with high-resolution SIMS measurements, we can determine the absolute $\delta^{11}B$ composition of COC, which reveals much lighter $\delta^{11}B$ values as low as ~17‰ (Fig. 5). The theca wall gives a highly consistent value of ~26‰ by both methods, confirming on one hand the reliability of our measurements, and on the other the fact that it is possible to isolate the $\delta^{11}B$ of theca by bulk (micromilling) approaches. A strong linear correlation is apparent between boron content and $\delta^{11}B$ (Fig. 5), indicating that the boron systematics of *L. pertusa* microstructures could vary as a function of the calcifying fluid pH. In effect, the local seawater pH at the Lopphavet reef is around 8.16 (Raddatz et al., 2016), implying a corresponding $\delta^{11}B$ of borate of 17‰, which is also the lowest measured value in the COC by SIMS. This may suggest that early biomineralisation of COC's potentially occurs directly from seawater, and that negligible biologically driven pH up-regulation and hence isotopic fractionation of borate occurs during calcification. Moreover, it implies that the borate ion is almost exclusively incorporated into the skeleton, which has been a subject of debate in recent years. Although significant quantities of boric acid have been reported (Klochko et al., 2009; Rollion-Bard et al., 2011), it has been argued that substantial incorporation of the trigonal species into the skeletal structures is unlikely as it would shift the $\delta^{11}B$ composition to considerably heavier values than those observed (McCulloch et al., 2012b; Wall et al., 2015). While the potential role of boric acid on the $\delta^{11}B$ composition of corals remains enigmatic, at present all points towards our $\delta^{11}B$ values being consistent with the direct uptake of the borate species.

Assuming inorganic boron fractionation during calcification, the internal $\delta^{11}B$ variations should reflect the pH at precipitation. From the distinct $\delta^{11}B$-pH values recorded in the COC and theca, we can therefore contemplate the different mechanisms responsible for biomineralisation of these structural domains. While the early COC zones seem to precipitate at normal pH range close to seawater (~8), secondary growth of aragonite crystals that characterises the theca wall occurs at elevated pH (up to ~9). At normal seawater pH (~8) bicarbonate ($HCO_3^-$) is the dominant DIC species available for calcification. Direct synthesis of this substrate would pose an efficient mechanism for calcification. This is generally assumed to occur via carbonic anhydrases, a group of enzymes well known to be involved in controlled biomineralisation processes of numerous animal taxa (e.g. Müller et al., 2013; Yu et al., 2006) as well as microbially-mediated carbonate formation (Krause et al., 2018). These ubiquitous enzymes have a significant catalytic activity for the physiological reaction of $CO_2$ hydration to bicarbonate (Moya et al., 2008). Plausibly, *L. pertusa* employs bicarbonate as the DIC source at the site of calcification, which is subsequently transported by calcifying cells (Tambutté et al., 2007). The final precipitation of carbonate ions ($CO_3^{2-}$) then follows at elevated pH. Up-regulation of calcifying fluid pH shifts the $HCO_3^-/CO_3^{2-}$ equilibrium enhancing the carbonate ion concentration, which is approximately an order of magnitude lower than calcium and enables the completion of the calcification reaction $Ca^{2+} + CO_3^{2-} = CaCO_3$.

### 4.2. Implications for proxy applications

The consistency of data determined from bulk subsampling and SIMS, together with the minimal internal $\delta^{11}B$ variations in the theca wall identified by SIMS, suggest that it is potentially suitable for proxy applications (Table 1 and Fig. 4). Moreover, our results indicate that $\delta^{11}B$ values of theca remain uniform among individuals from regimes of similar seawater pH (between approximately 8–8.16; Raddatz et al., 2016) across a wide geographical range and encompassing different environmental settings. For example, *L. pertusa* in the Oslofjord are subjected to rather extreme conditions and seasonal variations (Guihen et al., 2012) due to brackish seawater input from the Baltic Sea. In contrast, Lopphavet presents the northernmost flourishing reef at the verge of the North Atlantic Current system and Arctic waters. This suggests the theca wall to be a particularly valuable and robust skeletal structure for investigating $\delta^{11}B$-pH relationships, as it apparently is not significantly influenced by other confounding parameters. A prerequisite for its use in pH-proxy applications, nevertheless, is that a dependency of theca $\delta^{11}B$ and seawater-pH exists, for which a relevant calibration can be established. In the light of the previously discussed mechanisms controlling the formation of the theca aragonite (Section 4.1), the most likely underlying mechanism for such dependency would be that the $\delta^{11}B$ of theca reflects the optimal up-regulated pH, which is systematically impacted by decreasing seawater pH. A recent study, however, showed that *L. pertusa* maintains similar $\delta^{11}B$, and thus calcifying fluid pH, even under low pH conditions (Wall et al., 2015). These authors suggest that differences in food supply between the experimental treatments versus natural environment might explain the

lack of sensitivity to changes in seawater pH. Thus, processes controlling the up-regulation of calcifying fluid pH in *L. pertusa* may bear some similarities with shallow water (zooxanthellae bearing) *Porites* corals, which calcifying fluid pH (as well as DIC) was observed to strongly correlate with seasonal changes (McCulloch et al., 2017). This may suggest that even in the considerably colder deep-sea environments inhabited by *L. pertusa*, the ability of a coral to up-regulate is linked to energy/food requirements (Wall et al., 2015). Even though the apparent lack of sensitivity to pH might discourage the usefulness of *L. pertusa* as a pH archive at a first sight, a re-assessment considering a broader pH range (> 0.2–0.3 ΔpH), prolonged acidification (> 6 months), and improved analytical precision (solution-based $\delta^{11}B$ bulk measurements combined with B/Ca) with special focus on the composition of theca wall would help to reconcile these issues.

The potential use of theca material for proxy applications is further illustrated from the results obtained in the fossil samples (Table 1). Whilst recent samples provide essentially the same $\delta^{11}B$ values (26.5–26.8‰), fossil specimens differ considerably from modern values by up to 1.5‰. Higher $\delta^{11}B$ values of ~27.4‰ were recorded during the Late Pleistocene (~104 ka BP) in the sample from Challenger Mound off Ireland (Raddatz et al., 2014b), whereas the mid Holocene (~4.6 ka BP) $\delta^{11}B$ values were lower, ~25.1‰ measured in *L. pertusa* from Oslofjord. Providing that $\delta^{11}B$ of theca positively correlates with $\delta^{11}B$ of seawater, this would indicate that compared to modern oceans, seawater pH was elevated in the Late Pleistocene but lower during the Holocene. Alternatively, these data can be interpreted in the context of physiological pH modulation. Consequently, greater up-regulation might have been required due to potentially thermodynamically unfavourable conditions for carbonate skeleton formation during the Late Pleistocene, while up-regulation might not have been necessary during mid Holocene when the conditions for calcification were likely optimal. This would then imply a reverse trend, with relatively lower pH during the colder Late Pleistocene and higher pH in the warmer Holocene, and a positive dependence on temperature. In the Late Pleistocene, the onset of the last Weichselian glaciation was characterised by large ice sheets extending beyond the Scandinavian Mountains. Specifically, our sample corresponds to Marine Isotope Stage (MIS) 5c (93–105 ka). This period marks the initiation of long-term cooling associated with the decline in northern summer insolation due to changes in orbital forcing. In contrast, the mid Holocene is believed to have been generally warmer than today in the Northern Hemisphere, known also as the Holocene Climatic Optimum. Although a trend towards higher pH with glaciation is expected, Heinrich events for instance would have resulted in substantial melt-water input and so could also potentially lead to decreased pH. Moreover, atmospheric $CO_2$ and hence seawater $CO_3^{2-}$ were similar for both periods (Yu et al., 2013), which further complicates inferences on the measured $\delta^{11}B$ in the context of pH changes. At present, we can only speculate on the interpretation of these single $\delta^{11}B$ data points, and await more complete records from each site to deconvolve the relationship between the deep ocean carbonate system and carbon cycle. Despite these still unresolved complexities in the application of the $\delta^{11}B$-pH proxy in *L. pertusa*, our findings demonstrate that the $\delta^{11}B$ composition of theca wall does indeed vary on different timescales and is a promising target for palaeo-pH applications.

The ultimate uncertainty typically linked to palaeo-pH reconstructions is the role of post-depositional diagenesis that could alter the primary chemical signals in the carbonate archive. In marine conditions, early diagenesis is expected to lead to dissolution of primary aragonite and/or recrystallization of the secondary aragonite (Bar-Matthews et al., 1992; Gaillardet and Allègre, 1995; Allison et al., 2007). Providing that secondary aragonite precipitates in a fossil *L. pertusa* specimen, its formation would most probably occur from a solution of ranging $\delta^{11}B$ composition between the reef pore fluid and seawater (approximately between 17 and 40‰, respectively; taking the lowest measured value in *L. pertusa* as the minimum). Accordingly, recrystallised corals would be expected to have overall heavier $\delta^{11}B$ values. The broad internal variations, as observed in recent specimens (up to 10‰), may however complicate the identification of $\delta^{11}B$-specific diagenetic influences from the composition alone. A possible hypothesis could be that altered specimens will be expected to contain minimal internal heterogenities, as these would have been overridden by diagenesis. In particular, the skeletal areas characteristic of lower $\delta^{11}B$ values (such as COC's) will be likely considerably heavier and closer to the composition of theca. Providing that this is the case it puts another argument forward on the use of theca wall as the most robust and appropriate skeletal component for palaeo-proxy applications. In fact, assuming that the overall reduced intraskeletal $\delta^{11}B$ variations in the fossil *L. pertusa* from Lophhavet result from diagenetic alterations (Fig. 6), we still do not find large differences in the $\delta^{11}B$ composition of the theca between the fossil and the recent specimen (26.1 and 26.6‰, respectively; Table 1), further supporting this hypothesis. Regardless, a comprehensive understanding of the natural $\delta^{11}B$ and B/Ca variations in *L. pertusa* is essential, before specific skeletal compositions can be ascribed to diagenetic influences from geochemical data alone.

### 4.3. Integrated $\delta^{11}B$ approach

By combining bulk solution-based and *in situ* (SIMS and laser ablation) approaches, we can obtain a more complete picture of $\delta^{11}B$ variations within single specimens. While bulk and SIMS absolute $\delta^{11}B$ values of theca and the general offsets between microstructures appear to agree very well (within the resolution and analytical limitations of these techniques; Fig. 5), the laser measurements reveal different $\delta^{11}B$ compositions and trends, although the relative (large) amplitude in $\delta^{11}B$ is similar to the SIMS data (Fig. 6). Presumably these discrepancies between laser vs. bulk and SIMS can be linked to the differences between the techniques and the sample preparation protocols. Solution-based measurements are performed on a carefully milled bulk powder material from specific skeletal zones that undergoes rigorous cleaning procedures during which the organic material and stains are oxidised and removed. SIMS, on the other hand, requires highly polished surfaces, and the ion spots are typically highly selectively placed in optimal dense and structurally homogenous carbonate, combining a high spatial resolution (10 to 20 μm) with sub-μm depth integration to almost surface restricted analyses. In contrast to these methods, the laser ablates the complete surface to a depth, usually to an aspect ratio of one that includes pore spaces (and associated content), which is altogether analysed. Hence, laser measurements do not differentiate between the distinct components such as inclusions, organics, and carbonate material. Generally, the $\delta^{11}B$ values measured by laser were systematically lower in $\delta^{11}B$, which could indicate the presence of an additional source enriched in $^{10}B$, potentially lost or removed by the cleaning protocols for solution and SIMS procedures, or alternatively analytical issues that are yet to be identified. Although it is an important challenge to diagnose the origin of this offset, providing that it remains relatively constant, as in the present case, a simple correction would resolve the issue in first approximation.

Notably, the $\delta^{11}B$ composition of the fossil and the modern coral from Lopphavet measured by laser varied, with generally lower values found in the recent sample in contrast to the fossil (Fig. 6). Plausibly, this difference could be attributed to an additional light boron source originating from metastable components that may degrade during cleaning or by aging and diagenesis. Organic components, for instance, could be expected to degrade with time, which would result in heavier $\delta^{11}B$ values in fossil samples, such as observed here. Clearly, it is not straightforward to reconcile the differences in the $\delta^{11}B$ values measured between these approaches because of the different spatial scales and inherent biases arising from diverse sample preparation strategies. Nevertheless, only by comparing different methodologies can we hope to fully understand the $\delta^{11}B$ systematics of *L. pertusa*, and with it improve our understanding of past ocean and climate changes.

## 5. Conclusions

In summary, our study provides new insights into $\delta^{11}B$ variability in the deep-sea scleractinian coral *L. pertusa*. We identify large internal heterogeneities between structural zones characteristic of different biomineralisation mechanisms that operate within these domains; the early mineralising zones including COC's and septa, versus the more fibrous aragonite crystals dominating the theca wall. By combining multiple methods including solution-based micro-bulk analyses and high spatial resolution *in situ* SIMS and laser approaches, we find that the maximum relative difference in $\delta^{11}B$ is ~10‰. This could be potentially driven by two calcifying fluid pH end-members – a fluid of seawater like pH where the early mineralisation occurs, and a fluid with up-regulated pH that controls the precipitation during the secondary growth of aragonite crystals, in agreement with the two-step growth mode model. The full range of internal heterogeneities can only be evaluated using high spatial resolution techniques, as it is not feasible to isolate the pure COC fraction by micro-bulk sampling (micromilling). Conversely, the $\delta^{11}B$ composition of theca wall aragonite is very homogenous, with highly consistent values obtained by the different approaches. This suggests the theca material the most suitable skeletal structure for proxy-applications, providing that future studies can quantify the factors controlling the relationship between theca $\delta^{11}B$ and ambient seawater pH.

## Acknowledgements

This study is mainly based on material retrieved during research expedition with RV Poseidon (POS 391) realized by the DFG project RI 598/4-1. We thank the captain, crew, chief scientist Armin Form, and the scientific party of POS 391, with special thanks to the JAGO team – Karen Hissmann und Jürgen Schauer. We are grateful to Johanna Järnegren (from Norwegian Institute for Nature Research, Trondheim) for the support and samples from Trondheimsfjord. This project has received funding from the European Union's Horizon 2020 research and innovation programme under the Marie Sklodowska-Curie grant agreement No. 643084 (BASE-LiNE Earth) and the collaborative research initiative CHARON (DFG Forschergruppe 1644 - Phase II) funded by the German Research Foundation. J.R. acknowledges funding from DFG project ISOLDE DU 45/1 and 45/3 and ECHO RA 2156/1. J.T. and M.M. are supported by the Australian Research Council fellowship FL120100049, CE140100020 and acknowledge support from research project DP0986505.

## References

Adkins, J.F., Henderson, G.M., Wang, S.-L., O'Shea, S., Mokadem, F., 2004. Growth rates of the deep-sea scleractinia *Desmophyllum cristagallii* and *Enallopsammia rostrata*. Earth Planet. Sci. Lett. 227, 481–490.

Al-Horani, F.A., Al-Moghrabi, S.M., de Beer, D., 2003. The mechanism of calcification and its relation to photosynthesis and respiration in the scleractinian coral *Galaxea fascicularis*. Mar. Biol. 142, 419–426.

Allison, N., Finch, A.A., Webster, J.M., Clague, D.A., 2007. Palaeoenvironmental records from fossil corals: the effects of submarine diagenesis on temperature and climate estimates. Geochim. Cosmochim. Acta 71, 4693–4703.

Anagnostou, E., Huang, K.F., You, C.F., Sikes, E.L., Sherrell, R.M., 2012. Evaluation of boron isotope ratio as a pH proxy in the deep sea coral *Desmophyllum dianthus*: evidence of physiological pH adjustment. Earth Planet. Sci. Lett. 349, 251–260. https://doi.org/10.1016/j.epsl.2012.07.006.

Bar-Matthews, M., Wasserburg, G.J., Chen, J.H., 1992. Diagenesis of fossil coral skeletons: Correlation between trace elements, textures and $^{234}U/^{238}U$. Geochim. Cosmochim. Acta 57, 257–276.

Bates, N.R., Mathis, J.T., 2009. The Arctic Ocean marine carbon cycle: evaluation of air-sea $CO_2$ exchanges, ocean acidification impacts and potential feedbacks. Biogeosciences 6, 2433–2459.

Blamart, D., Rollion-Bard, C., Meibom, A., Cuif, J.-P., Juillet-Leclerc, A., Dauphin, Y., 2007. Correlation of boron isotopic composition with ultrastructure in the deep-sea coral *Lophelia pertusa*: Implication for biomineralization and paleo-pH. Geochem. Geophys. Geosyst. 8, 1525–2027.

Büscher, J., Form, A.U., Riebesell, U., 2017. Interactive effects of ocean acidification and warming on growth, fitness, and survival of the cold-water coral *Lophelia pertusa* under different food availabilities. Front. Mar. Sci. 4, 101.

Büttner, S.H., Reid, W., Glodny, J., Wiedenbeck, M., Chuwa, G., Moloto, T., Gucsik, A., 2016. Fluid sources in the Twangiza-Namoya Gold Belt (Democratic Republic of Congo): evidence from tourmaline and fluid compositions, and from boron and Rb-Sr isotope systematics. Precambrian Res. 280, 161–178.

Caldeira, K., Wickett, M.E., 2003. Anthropogenic carbon and ocean pH. Nature 425, 365.

Catanzaro, E.J., Champion, C.E., Garner, E.L., Marinenko, G., Sappenfield, K.M., Shields, W.R., 1970. Standard Reference Materials: Boric Acid; Isotopic and Assay Standard Reference Materials. US National Bureau of Standards, Special Publication (260-17).

Cohen, A.L., Gaetani, G.A., Lundälv, T., Corliss, B.H., George, R.Y., 2006. Compositional variability in a cold-water scleractinian, *Lophelia pertusa*: New insights into "vital effects". Geochem. Geophys. Geosyst. 7, 1525–2027.

Cuif, J.-P., Dauphin, Y., 2005. The two-step mode of growth in the scleractinian coral skeletons from the micrometer to the overall scale. J. Struct. Biol. 150, 319–331.

Dickson, A.G., 1990. Thermodynamics of the dissociation of boric-acid in synthetic seawater from 273.15-k to 318.15-k. Deep-Sea Res. A, Oceanorg. Res. Pap. 37, 755–766. https://doi.org/10.1016/0198-0149(90)90004- F.

Dorschel, B., Hebbeln, D., Rüggeberg, A., Dullo, W.-C., Freiwald, A., 2005. Growth and erosion of a cold-water coral covered carbonate mound in the Northeast Atlantic during the Late Pleistocene and Holocene. Earth Planet. Sci. Lett. 233, 33–44.

Douville, E., Paterne, M., Cabioch, G., Louvat, P., Gaillardet, J., Juillet-Leclerc, A., Ayliffe, L., 2010. Abrupt sea surface pH change at the end of the Younger Dryas in the central sub-equatorial Pacific inferred from boron isotope abundance in corals (*Porites*). Biogeosciences 7, 2445–2459.

Fietzke, J., Heinemann, A., Taubner, I., Böhm, F., Erez, J., Eisenhauer, A., 2010. Boron isotope ratio determination in carbonates via LA-MC-ICP-MS using soda-lime glass standards as reference material. J. Anal. At. Spectrom. 25, 1953–1957.

Fietzke, J., Ragazzola, F., Halfar, J., Dietze, H., Foster, L.C., Hansteen, T.H., Eisenhauer, A., Steneck, R.S., 2015. Century-scale trends and seasonality in pH and temperature for shallow zones of the Bering Sea. Proc. Natl. Acad. Sci. 112, 2960–2965.

Flögel, S., Dullo, W.-C., Pfannkuche, O., Kiriakoulakis, K., Rüggeberg, A., 2014. Geochemical and physical constraints for the occurrence of living cold-water corals. Deep Sea Res., Part II 99, 19–26. https://doi.org/10.1016/j.dsr2.2013.06.006.

Foster, G.L., Pogge von Strandmann, P.A.E., Rae, J.W.B., 2010. Boron and magnesium isotopic composition of seawater. Geochem. Geophys. Geosyst. 11, Q08015. https://doi.org/10.1029/2010GC003201.

Freiwald, A., Fosså, J.H., Grehan, A., Koslow, T., Roberts, J.M., 2004. Cold-Water Coral Reefs. UNEP-WCMS, Cambridge, UK.

Gaillardet, J., Allègre, C.J., 1995. Boron isotopic composition of corals: Seawater or diagenesis record? Earth Planet. Sci. Lett. 136, 665–676.

Gass, S.E., Roberts, J.M., 2011. Growth and branching patterns of *Lophelia pertusa* (Scleractinia) from the North Sea. J. Mar. Biol. Assoc. UK 91, 831–835.

Guihen, D., White, M., Lundälv, R., 2012. Temperature shocks and ecological implication at a cold-water coral reef. Mar. Biodiv. Rec. 5, 1–10.

Guinotte, J.M., Orr, J., Cairns, S., Freiwald, A., Morgan, L., George, R., 2006. Will human-induced changes in seawater chemistry alter the distribution of deep-sea scleractinian corals? Front. Ecol. Environ. 4, 141–146.

Halloran, P.R., Booth, B.B.B., Jones, C.D., Lambert, F.H., McNeall, D.J., Totterdell, I.J., Völker, C., 2015. The mechanisms of North Atlantic $CO_2$ uptake in a large Earth System Model ensemble. Biogeosciences 12, 4497–4508.

Hemming, N.G., Hanson, G.N., 1992. Boron isotopic composition and concentration in modern marine carbonates. Geochim. Cosmochim. Acta 56, 537–543.

Henehan, M.J., Foster, G.L., Bostock, H.C., Greenop, R., Marshall, B.J., Wilson, P.A., 2016. A new boron isotope-pH calibration for *Orbulina universa*, with implication for understanding and accounting for 'vital effects'. Earth Planet. Sci. Lett. 454, 282–292.

Hönisch, B., Bijima, J., Russell, A.D., Spero, H.J., Palmer, M.R., Zeebe, R.E., Eisenhauer, A., 2003. The influence of symbiont photosynthesis on the boron isotopic composition of foraminifera shells. Mar. Micropaleontol. 49, 87–96.

Hönisch, B., Hemming, N.G., Grottoli, A.G., Amat, A., Hanson, G.N., Bijima, J., 2004. Assessing scleractinian corals as recorders for paleo-pH: Empirical calibration and vital effects. Geochim. Cosmochim. Acta 68, 3675–3685.

Houlbrèque, F., McCulloch, M., Roark, B., Guilderson, T., Meibom, A., Kimball, J., Mortimer, G., Cuif, J.-P., Dunbar, R., 2010. Uranium-series dating and growth characteristics of the deep-sea scleractinian coral: *Enallopsammia rostrata* from the Equatorial Pacific. Geochim. Cosmochim. Acta 74, 2380–2395.

IPCC, 2013. In: Stocker, T.F., Qin, D., Plattner, G.-K., Tignor, M., Allen, S.K., Boschung, J., Nauels, A., Xia, Y., Bex, V., Midgley, P.M. (Eds.), Climate Change 2013: The Physical Science Basis. Contribution of Working Group I to the Fifth Assessment Report of the Intergovern- mental Panel on Climate Change. Cambridge University Press, Cambridge, United Kingdom and New York, NY, USA, pp. 1535.

Jurikova, H., Liebetrau, V., Gutjahr, M., Rollion-Bard, C., Hu, M.Y., Krause, S., Henkel, D., Hiebenthal, C., Schmidt, M., Laudien, J., Eisenhaer, A., 2019. Boron isotope systematics of cultured brachiopods: response to acidification, vital effects and implications for palaeo-pH reconstruction. Geochim. Cosmochim. Acta. https://doi.org/10.1016/j.gca.2019.01.015. (in press).

Kaczmarek, K., Nehrke, G., Misra, S., Bijima, J., Elderfield, H., 2016. Investigating the effects of growth rate and temperature on the B/Ca ratio and $\delta^{11}B$ during inorganic calcite formation. Chem. Geol. 421, 81–92.

Kasemann, S.A., Schmidt, D.N., Bijima, J., Foster, G.L., 2009. *In situ* boron isotope analyses in marine carbonates and its application for foraminifera and palaeo-pH. Chem. Geol. 260, 138–147.

Klochko, K., Kaufman, A.J., Wengsheng, Y., Byrne, R.H., Tossell, J.A., 2006. Experimental measurement of boron isotope fractionation in seawater. Earth Planet. Sci. Lett. 248, 276–285.

Klochko, K., Cody, G.D., Tossell, J.A., Dera, P., Kaufman, A.J., 2009. Re-evaluating boron speciation in biogenic calcite and aragonite using $^{11}B$ MAS NMR. Geochim.

Cosmochim. Acta 73, 1890–1900.
Krause, S., Liebetrau, V., Löscher, C.R., Böhm, F., Gorb, S., Eisenhauer, A., Treude, T., 2018. Marine ammonification and carbonic anhydrase activity induce rapid calcium carbonate precipitation. Geochim. Cosmochim. Acta (accepted).
Krief, S., Hendy, E.J., Fine, M., Yam, R., Meibom, A., Foster, G.L., Shemesh, A., 2010. Physiological and isotopic responses of scleractinian corals to ocean acidification. Geochim. Cosmochim. Acta 74, 4988–5001.
Liu, Y., Liu, W., Peng, Z., Xiao, Y., Wei, G., Sun, W., He, J., Liu, G., Chou, C.-L., 2009. Instability of seawater pH in the South China Sea during the mid-late Holocene: evidence from boron isotopic composition of corals. Geochim. Cosmochim. Acta 73, 1264–1272.
Martínez-Botí, M.A., Marino, G., Foster, G.L., Ziveri, P., Henehan, M.J., Rae, J.W.B., Mortyn, P.G., Vance, D., 2015. Boron isotope evidence for oceanic carbon dioxide leakage during the last deglaciation. Nature 518, 219–222.
Marubini, F., Ferrier-Pagès, C., Furla, P., Allemand, D., 2008. Coral calcification responds to seawater acidification: a working hypothesis towards a physiological mechanism. Coral Reefs 27, 491–499.
McCulloch, M., Falter, J., Trotter, J., Montagna, P., 2012a. Coral resilience to ocean acidification and global warming through pH up-regulation. Nat. Clim. Chang. 2, 623–627.
McCulloch, M., Trotter, J., Montagna, P., Falter, J., Dunbar, R., Freiwald, A., Försterra, G., López, Correa M., Maier, C., Rüggeberg, A., Taviani, M., 2012b. Resilience of cold-water scleractinian corals to ocean acidification: Boron isotopic systematics of pH and saturation state up-regulation. Geochim. Cosmochim. Acta 87, 21–34.
McCulloch, M.T., Holcomb, M., Rankenburg, K., Trotter, J.A., 2014. Rapid, high-precision measurements of boron isotopic compositions in marine carbonates. Rapid Commun. Mass Spectrom. 28, 2704–2712. https://doi.org/10.1002/rcm.7065.
McCulloch, M.T., D'Olivo, J.P., Falter, J., Holcomb, M., Trotter, J., 2017. Coral calcification in a changing World and the interactive dynamics of pH and DIC upregulation. Nat. Commun. 8, 15686.
Meibom, A., Yurimoto, H., Cuif, J.-P., Domart-Coulon, I., Houlbrèque, F., Constantz, B., Dauphin, Y., Tambutté, E., Tambutté, S., Allemand, D., Wooden, J., Dunbar, R., 2006. Vital effects in coral skeleton display strict three-dimensional control. Geophys. Res. Lett. 33, L11608. https://doi.org/10.1029/2006GL025968.
Millero, F.J., 1979. The thermodynamics of the carbonate system in seawater. Geochim. Cosmochim. Acta 43, 1651–1661.
Montagna, et al., 2014. Li/Mg systematics in scleractinian corals: Calibration of the thermometer. Geochim. Cosmochim. Acta 132, 288–310.
Moya, A., Tambutté, S., Bertucci, A., Tambutté, E., Lotto, S., Vullo, D., Supuran, C.T., Allemand, D., Zoccola, D., 2008. Carbonic anhydrase in the Scleractinian coral *Stylophora pistillata*. J. Biol. Chem. 283, 25475–25484.
Müller, W.E.G., Schröder, H.C., Schlossmacher, U., Neufurth, M., Geurtsen, W., Korzhev, M., Wang, X., 2013. The enzyme carbonic anhydrase as an integral component of biogenic Ca-carbonate formation in sponge spicules. FEBS Open Bio 3, 357–365. https://doi.org/10.1016/j.fob.2013.08.004.
Nir, O., Vengosh, A., Harkness, J.S., Dwyer, G., Lahav, O., 2015. Direct measurement of the boron isotope fractionation factor: reducing the uncertainty in reconstructing ocean paleo-pH. Earth Planet. Sci. Lett. 414, 1–5.
Okai, T., Suzuki, A., Kawahata, H., Terashima, S., Imai, N., 2002. Preparation of a New Geological Survey of Japan Geochemical Reference Material: Coral JCp- 1. Geostand. Geoanal. Res. 26, 95–99.
Orr, J.C., et al., 2005. Anthropogenic ocean acidification over the twenty-first century and its impact on calcifying organisms. Nature 437, 681–686.
Raddatz, J., et al., 2013. Stable Sr-isotope, Sr/Ca, Mg/Ca, Li/Ca and Mg/Li ratios in the scleractinian cold-water coral *Lophelia pertusa* 2013. Chem. Geol. 352, 143–152.
Raddatz, J., Rüggeberg, A., Flögel, S., Hathorne, E., Liebetrau, V., Eisenhauer, A., Dullo, W.-C., 2014a. The influence of seawater pH on U/Ca ratios in the scleractinian cold-water corals *Lophelia pertusa*. Biogeosciences 11, 1863–1871. https://doi.org/10.5194/bg-11-1863-2014.
Raddatz, J., Rüggeberg, A., Liebetrau, V., Foubert, A., Hathorne, E.C., Fietzke, J., Eisenhauer, A., Dullo, W.-C., 2014b. Environmental boundary conditions of cold-water coral mound growth over the last 3 million years in the Porcupine Seabight, Northeast Atlantic. Deep Sea Res., Part II 99, 227–236. https://doi.org/10.1016/j.dsr2.2013.06.009.
Raddatz, J., Liebetrau, V., Trotter, J., Rüggeberg, A., Flögel, S., Dullo, W.-C., Eisenhauer, A., Voigt, S., McCulloch, M., 2016. Environmental constraints on Holocene cold-water coral reef growth off Norway: insights from a multiproxy approach. Paleoceanography 31, 1350–1367. https://doi.org/10.1002/2016PA002974.
Rae, J.W.B., Foster, G.L., Schmidt, D.N., Elliott, T., 2011. Boron isotopes and B/Ca in benthic foraminifera: proxies for the deep ocean carbonate system. Earth Planet. Sci. Lett. 302, 403–413.
Rasbury, E.T., Hemming, N.G., 2017. Boron isotopes: a 'Paleo-pH Meter' for tracking ancient atmospheric $CO_2$. Elements 13, 243–248.
Ries, J.B., 2011. A physicochemical framework for interpreting the biological calcification response to $CO_2$-induced ocean acidification. Geochim. Cosmochim. Acta 75, 4053–4064.
Roberts, J.M., Wheeler, A.J., Freiwald, A., 2006. Reefs of the deep: the biology and geology of cold-water coral ecosystems. Science 312, 543–547.
Rollion-Bard, C., Blamart, D., Cuif, J.-P., Dauphin, Y., 2010. *In situ* measurements of oxygen isotopic composition in the deep-sea coral *Lophelia pertusa*: Re-examination of the current geochemical models of biomineralisation. Geochim. Cosmochim. Acta 74, 1338–1349.
Rollion-Bard, C., Blamart, D., Trebosc, J., Tricot, G., Mussi, A., Cuif, J.-P., 2011. Boron isotopes as pH proxy: a new low at boron speciation in the deep-sea corals using $^{11}B$ MAS NMR and EELS. Geochim. Cosmochim. Acta 75, 1003–1012.
Rüggeberg, A., Fietzke, J., Liebetrau, V., Eisenhauer, A., Cullo, W.-C., Freiwald, A., 2008. Stable strontium isotopes ($\delta^{88/86}Sr$) in cold-water corals – a new proxy for reconstruction of intermediate ocean water temperatures. Earth Planet. Sci. Lett. 269, 570–575.
Sanyal, A., Nugent, M., Reeder, R.J., Bijima, J., 2000. Seawater pH control on the boron isotopic composition of calcite: evidence from inorganic calcite precipitation experiments. Geochim. Cosmochim. Acta 64, 1551–1555.
Schlitzer, R., 2016. Ocean Data View. http://odv.awi.de.
Silverman, J., Lazar, B., Cao, L., Caldeira, K., Erez, J., 2009. Coral reefs may start dissolving when atmospheric $CO_2$ doubles. Geophys. Res. Lett. 36, L05606. https://doi.org/10.1029/2008GL036282.
Stewart, J.A., Anagnostou, E., Foster, G.L., 2016. An improved boron isotopes pH proxy calibration for the deep-sea coral *Desmophyllum dianthus* through sub-sampling of fibrous aragonite. Chem. Geol. 447, 148–160.
Tambutté, S., Tambutté, E., Zoccola, D., Caminiti, N., Lotto, S., Moya, A., Allemand, D., Adkins, J., 2007. Characterisation and role of carbonic anhydrase in the calcification process of the azooxanthellate coral *Tubastrea aurea*. Mar. Biol. 151, 71–83.
Tanaka, K., Holcomb, M., Takahashi, A., Kurihara, H., Asami, R., Shinjo, R., Sowa, K., Rankenburg, K., Watanabe, T., McCulloch, M., 2015. Response of *Acropora digitifera* to ocean acidification: constrains from $\delta^{11}B$, Sr, Mg, and Ba compositions of aragonitic skeletons cultured under variable seawater pH. Coral Reefs 34, 1139–1149.
Trotter, J., Montagna, P., McCulloch, M., Silenzi, S., Reynaud, S., Mortimer, G., Martin, S., Ferrier-Pagès, C., Gattuso, J.-P., Rodolfo-Metalpa, R., 2011. Quantifying the pH 'vital effect' in the temperate zooxanthellate coral *Cladocora caespitosa*: Validation of the boron seawater pH proxy. Earth Planet. Sci. Lett. 303, 163–173.
Uchikawa, J., Penman, D.E., Zachos, J.C., Zeebe, R.E., 2015. Experimental evidence for kinetic effects on B/Ca in synthetic calcite: implications for potential $B(OH)_4^-$ and $B(OH)_3$ incorporation. Geochim. Cosmochim. Acta 150, 171–191.
Vengosh, A., Kolodny, Y., Starinsky, A., Chivas, A.R., McCulloch, M.T., 1991. Coprecipitation and isotopic fractionation of boron in modern biogenic carbonates. Geochim. Cosmochim. Acta 55, 2901–2910.
Vielzeuf, D., Gagnon, A.C., Ricolleau, A., Devidal, J.-L., Balme-Heuze, C., Yahiaoui, N., Fonquernie, C., Perrin, J., Garrabou, J., Montel, J.-M., Floquet, N., 2018. Growth Kinetics and distribution of trace elements in precious corals. Front. Earth Sci. 6, 167.
Wall, M., Ragazzola, F., Foster, L.C., Form, A., Schmidt, D.N., 2015. pH up-regulation as a potential mechanisms for the cold-water coral *Lophelia pertusa* to sustain growth in aragonite undersaturated conditions. Biogeosciences 12, 6869–6880.
Wang, B.-S., You, C.-F., Huang, K.-F., Wu, S.-F., Aggarwal, S.K., Chung, C.-H., Lin, P.-Y., 2010. Direct separation of boron from Na- and Ca-rich matrices by submimation for stable isotope measurements by MC-ICP-MS. Talanta 82, 1378–1384.
Wei, G., McCulloch, M.T., Mortimer, G., Deng, W., Xie, L., 2009. Evidence for ocean acidification in the Great Barrier Reef of Australia. Geochim. Cosmochim. Acta 73, 2332–2346.
Yu, Z., Xie, L., Lee, S., Zhnag, R., 2006. A novel carbionic anhydrase from the mantle of the pearl oyster (*Pinctada funcata*). Comp. Biochem. Physiol. B 143, 190–194.
Yu, J., Anderson, R.F., Jin, Z., Rae, J.W.B., Opdyke, B.N., Eggins, S.M., 2013. Responses of the deep ocean carbonate system to carbon reorganization during the Last Glacial-interglacial cycle. Quat. Sci. Rev. 76, 39–52.
Zeebe, R.E., 2005. Stable boron isotope fractionation between dissolved $B(OH)_3$ and $B(OH)_4^-$. Geochim. Cosmochim. Acta 69, 2753–2766.